ELSEVIER

Journal of Fluids and Structures 23 (2007) 1215–1230

JOURNAL OF FLUIDS AND STRUCTURES

www.elsevier.com/locate/jfs

Large eddy simulation of cross-flow through a staggered tube bundle at subcritical Reynolds number

C. Liang, G. Papadakis*

Experimental and Computational Laboratory for the Analysis of Turbulence, Department of Mechanical Engineering, King's College London, Strand, WC2R 2LS, London, UK

Received 17 May 2005; accepted 3 May 2007
Available online 20 September 2007

Abstract

The Large Eddy Simulation (LES) technique is used to study the vortex shedding characteristics inside a staggered tube array consisting of six rows with intermediate spacings ($S_L/D \times S_T/D = 1.6 \times 3.6$) at the subcritical Reynolds number of 8600 (based on the gap velocity). The filtered equations are discretised using the finite volume method in an unstructured, collocated grid arrangement with second-order accurate methods in space and time. The predictions of mean velocities and Reynolds stresses are in very good agreement with detailed LDA measurements performed in 17 stations along the depth of the array. The sizes of the recirculation zones behind the cylinders in the first and third row also compare favourably with available correlations. Two distinct and independent shedding frequencies are detected behind the first two rows, but the high-frequency component vanishes in the downstream rows. The corresponding Strouhal numbers agree well with measurements available in the literature for similar tube spacings. The lift coefficient as well as instantaneous flow patterns of the whole array are also examined.

Keywords: Heat exchanger; Tube bundles; Large eddy simulation; Vortex shedding; Finite volume method; Unstructured grid

1. Introduction

Tube bundles are widely employed in cross-flow heat exchangers, the design of which is still based on empirical correlations of heat transfer and pressure drop which have limitations and are of doubtful accuracy. The shell-and-tube heat exchanger is the most versatile type of cross-flow exchangers (Kakac and Liu, 1997) and is the one most widely used in the process and power industries. In fact, it accounts for more that 85% of new heat exchangers supplied to the oil refining, chemical, petrochemical and power companies in leading European countries (Butterworth et al., 1996). Therefore, efficient design and operation of such equipment can lead to significant energy savings.

Apart from heat transfer considerations, the design also should account for vortex-induced vibrations. The instability of the shear layers and, most importantly, the large-scale vortex shedding as well as the different wake interaction mechanisms are factors that can lead to large-amplitude vibrations or structural resonance in the array and induce serious structural failure resulting in lost revenue and high repair costs. Consequently, reliable numerical methods for

*Corresponding author. Tel.: +44 207848 2049; fax: +44 207848 2932.
E-mail address: george.papadakis@kcl.ac.uk (G. Papadakis).

0889-9746/$ - see front matter
doi:10.1016/j.jfluidstructs.2007.05.004

the characterisation of existing (or the development of new) designs are urgently needed in order to avoid extensive and expensive experimentation.

There are two main types of tube array configurations: in-line and staggered. In the former type, one row of tubes is placed exactly behind the next along the streamwise direction, without displacement in the cross-flow direction (Ziada and Oengören, 1992, 1993; Konstantinidis et al., 2000). In staggered arrays, every second row of tubes is displaced resulting in several configurations: symmetric arrays (Balabani and Yianneskis, 1996, 1997), rotated square arrays (Simonin and Barcouda, 1988; Weaver et al., 1993; Price et al., 1995), normal triangle arrays (Polak and Weaver, 1995; Oengören and Ziada, 1998), parallel triangle arrays (Price et al., 1995; Ziada and Oengören, 2000), etc.

All the aforementioned studies are experimental and have revealed very complicated flow features. Even for two staggered circular cylinders in cross-flow, Sumner et al. (2000) identified nine different flow patterns depending on the centre-to-centre distance (pitch) and the angle of incidence with respect to the approaching flow. Complex flow field characteristics such as reattachment of shear layers, induced separation, vortex synchronisation and impingement or vortex pairing, splitting and enveloping were revealed. In multi-cylinder arrays with many rows, the flow patterns are even more complicated and difficult to characterise as the wakes are interacting. It is thus no surprise that multiple shedding frequencies have been found that depend on the flow velocity, the array configuration and, most importantly, the examined location inside the bundle. Oengören and Ziada (1998) investigated the vortex shedding characteristics inside several normal triangle tube arrays and found three vortex shedding frequencies for an array with pitch to diameter ratio equal to 2.08 for a range of $\mathrm{Re}_{\mathrm{gap}}$ (defined as $U_{\mathrm{gap}}D/\nu$) from 22 200 to 45 000. The high frequency was associated with the cylinders located in the first rows, the low one was associated with the downstream rows, while the third frequency was the result of the nonlinear interaction between these two and was exactly equal to their difference. They also demonstrated that the multiple frequency nature of vortex shedding in the first few cylinder rows depends strongly on the Reynolds number. For instance, if the Reynolds number increases above 45 000, the vortex shedding transforms into a single frequency event at the lower frequency. Polak and Weaver (1995) also studied normal triangular tube arrays in the Reynolds number range 760–49 000 (based on the upstream flow velocity) and found that for a pitch-to-diameter ratio greater than 2.0, the vortex shedding from the second row occurs at a lower frequency than that from the first row. Weaver et al. (1993) conducted wind tunnel experiments in rotated square arrays with pitch ratios from 1.21 to 2.83 and, except for the smallest pitch ratio array, they also identified two distinct shedding frequencies in the first and second tube rows. Two vortex shedding frequencies were also detected in the two-cylinder arrangements by Sumner et al. (2000). Their study revealed that the frequencies are associated with individual shear layers (rather than with individual cylinders) and found that the two shear layers from the downstream cylinder often shed vortices at different frequencies.

Against this background of detailed experimental investigations, most numerical simulations of the flow around tube bundles, until recently, lacked accurate predictive capability and therefore have not yet been employed for thorough, in-depth studies in order to understand and elucidate the aforementioned patterns. The vast majority of them are based on one (or more) of the following simplifying assumptions: two-dimensionality, low Reynolds number laminar flow, statistically steady turbulent flow or fully developed periodic flow in the streamwise and cross-stream direction. For higher Reynolds numbers, approaches that are based on the solution of the Reynolds Averaged Navier–Stokes (RANS) equations with a variety of turbulence models have been predominantly employed.

Recently, the first direct numerical simulations (DNS) in tube bundle flows appeared in the literature (Moulinec et al., 2004b). The Reynolds number (based on the bulk velocity) was equal to 6000 and the finest mesh had $196 \times 196 \times 128$ cells. The computational domain comprised only an elemental (or periodic) 'cell', assuming fully developed flow in the streamwise and cross-stream directions. The predictions compared well with the experiments of Simonin and Barcouda (1988) for both mean and r.m.s. velocities. DNS at various Reynolds numbers between 50 and 6000 and more elemental 'cells' were also reported by Moulinec et al. (2004a). Very interesting results on the wake disappearance were presented and compared with theoretical asymptotic limits for laminar and turbulent strained flows. However, information on vortex shedding was not reported in these papers.

The Large Eddy Simulation (LES) technique is situated between the RANS and DNS in the sense that large scales are calculated directly while the small ones are approximated. The fact that in tube bundles momentum and heat transfer are, to a large extent, controlled by large scale vortices shed behind the cylinders, makes this technique particularly attractive. The first simulations were two-dimensional (Hassan and Ibrahim, 1997; Barsamian and Hassan, 1997; Bouris and Bergeles, 1999; Hassan and Barsamian, 1999). However, the problem of two-dimensional LES calculations is that important mechanisms, such as vortex stretching, cannot be reproduced. Pioneering three-dimensional LES calculations inside a staggered tube bundle [studied experimentally by Simonin and Barcouda (1988)] were performed by Rollet-Miet et al. (1999) and Benhamadouche and Laurence (2003) using the finite element and finite volume methods, respectively. In both papers, the flow through an elemental 'cell' was simulated assuming periodicity in the streamwise and cross-stream directions and improved predictions compared to the RANS approach for mean and

turbulence quantities were reported. They also observed that the subgrid-scale model, whether the standard Smagorinsky with constant coefficient or the dynamic version, had little effect on the results. Hassan and Barsamian (2004) also studied with LES the same experimental arrangement. In contrast to the above investigators, they accounted for the flow development along multiple rows. The instantaneous vorticity contours revealed a clear shedding behind the tubes, but no further information was provided. It is likely that vortex shedding, although present, was not very strong for this particular tube bundle because of the close tube spacing; the tube arrangement corresponds to a rotated square array with a small pitch-to-diameter ratio (equal to 1.47).

The above literature survey indicates that detailed validation of the LES methodology in arrays with intermediate tube spacings (for which vortex shedding is strong) in terms of mean and turbulence quantities has yet to appear in the literature. Also, the capacity of this methodology to capture the multiple shedding frequencies measured experimentally has not been confirmed yet. In order to fill this gap, fully three-dimensional LES calculations over a number of rows in a staggered tube bundle with intermediate tube spacings are reported in this paper. The predictions are validated against detailed mean and r.m.s. velocity measurements as well as correlations for the length of recirculation zones. Instantaneous velocities are also recorded behind the tubes in order to study the vortex shedding characteristics.

The rest of the paper is arranged as follows. First, the geometry and computational conditions are presented followed by the modelling approach and the solution methodology. The predictions for mean and r.m.s. velocities (streamwise as well as cross-stream) are then validated against detailed experimental data. Following validation, instantaneous flow patterns are analysed and the associated Strouhal numbers are compared with available measurements from the literature.

2. Geometry and conditions

The configuration of the examined six-row staggered tube bundle, the tube spacings in the longitudinal (S_L) and transverse (S_T) directions, the size of the computational domain, the origin of the coordinate system as well as the tube (row) numbering convention are shown in Fig. 1. The domain is based on the experimental set-up of Balabani and Yianneskis (1996) with values $S_L \times S_T = 1.6D \times 3.6D$ for the longitudinal and transverse spacings, respectively. The experiments, against which the simulations are compared, were carried out in a stainless steel water tunnel with cross-section 72 mm × 72 mm. The computational domain is described in a fixed Cartesian coordinate system (x, y, z). The x-axis is along the streamwise (longitudinal) flow direction, the z-axis is parallel to the cylinder axis (spanwise direction), while the y-axis is perpendicular to both the x- and z-axis (transverse or cross-stream direction). Half-cylinders are fixed on the top and bottom walls to minimise boundary layer effects. The diameter of each cylinder is 10 mm. The bulk approaching velocity is 0.62 m/s and the gap velocity 0.86 m/s and the corresponding Reynolds numbers are equal to 6200 and 8600, respectively.

Across the entrance of the computational domain the velocity profile is assumed to be uniform and the turbulent intensity equal to zero. To account properly for the turbulence at the entrance would necessitate a separate LES simulation of a channel flow that would inevitably increase significantly the computational time of the whole

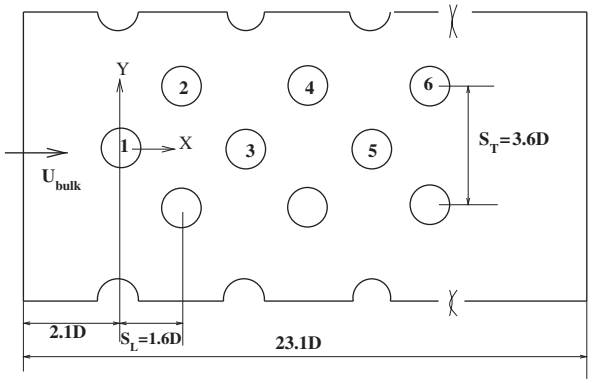

Fig. 1. Configuration of the six-row staggered tube array and tube (row) numbering.

simulation. A faster, but less rigorous, method to produce turbulent fluctuations is to use a zero mean Gaussian random distribution with the correct standard deviation. In that case, however, the fluctuations will not be temporally and spatially correlated. Note that this problem is entirely alleviated when the 'elemental cell' approach is used, as periodic conditions are used between inlet and outlet. For the examined arrangement the measured r.m.s. values normalised by the gap velocity at $x = 0$ are 6.25% and 4.29% for the streamwise and cross-stream velocities, respectively. As will be shown in the results section, the levels of r.m.s. velocities after the second row are significantly higher compared to these values which suggests that turbulence is generated mainly due to the presence of the cylinder walls and the vortex shedding processes behind the tubes. Therefore, inlet conditions are quickly overshadowed by turbulence generated downstream.

3. Modelling approach and solution method

Applying a low-pass spatial filter to the incompressible Navier–Stokes equations and assuming that the filtering and differentiation operations commute, the following equations written in tensorial Cartesian form, are obtained:

$$\frac{\partial \widetilde{u_i}}{\partial x_i} = 0, \tag{1}$$

$$\frac{\partial \widetilde{u_i}}{\partial t} + \frac{\partial \widetilde{u_i}\widetilde{u_j}}{\partial x_j} = -\frac{1}{\rho}\frac{\partial \widetilde{P}}{\partial x_i} - \frac{\partial \tau_{ij}}{\partial x_i} + \nu \frac{\partial^2 \widetilde{u_i}}{\partial x_j \partial x_j}, \tag{2}$$

where the index ($i = 1, 2, 3$) represents each direction in the Cartesian coordinate system while the tilde denotes filtered quantities. The subgrid-scale Reynolds stresses τ_{ij} are given by

$$\tau_{ij} = \widetilde{u_i u_j} - \widetilde{u_i}\widetilde{u_j}. \tag{3}$$

To model the above term, the standard Smagorinsky (1963) model was used. It has been found by Rollet-Miet et al. (1999) as well as Benhamadouche and Laurence (2003) that for the close-spaced tube array of Simonin and Barcouda (1988) at very similar Reynolds numbers to those in the present study, the effect of the subgrid-scale model is small. This finding is expected to be even more valid for the present configuration, as the tube spacings are larger and, as will be shown later on, there is significant vortex shedding activity behind each tube that is expected to dominate momentum transfer and thus minimise the effect of subgrid-scale stresses. The Smagorinsky model employs the Boussinesq approximation:

$$\tau_{ij} - \frac{\delta ij}{3}\tau_{kk} = -2\nu_T \widetilde{S_{ij}} = -\nu_T\left(\frac{\partial \widetilde{u_i}}{\partial x_j} + \frac{\partial \widetilde{u_j}}{\partial x_i}\right), \tag{4}$$

where $\widetilde{S_{ij}}$ is the resolved-scale strain rate tensor. The trace of the subgrid-scale stresses τ_{kk} is incorporated in the pressure resulting in a modified pressure term. The eddy viscosity is modelled as

$$\nu_T = (C_s \Delta)^2 |\widetilde{S}|. \tag{5}$$

Using the Kolmogorov spectrum Lilly (1977) showed that the value of the Smagorinsky constant C_s for high-Reynolds number turbulence in local equilibrium (i.e. when the transfer of energy to the residual motions is balanced by dissipation) is equal to 0.17. However, several investigators (Deardorff, 1970; Piomelli et al., 1988) have found that in the presence of shear this value must be reduced to around 0.1 and this value is used in the present investigation. More information about the Smagorinsky model and constant can be found in the book of Sagaut (2002). The magnitude of the strain rate tensor $|\widetilde{S}|$ is $\sqrt{2\widetilde{S_{ij}}\widetilde{S_{ij}}}$. The filter length Δ is evaluated using $\Delta = (\mathrm{Vol})^{1/3}$ where Vol is the volume of the computational cell.

The finite volume method applied on an unstructured, collocated grid arrangement is employed to discretise the governing equations. All spatial terms in the momentum equations are discretised using the second-order central differencing scheme (CDS) while the second order accurate Crank–Nicolson method is employed to advance them in time, with the exception of the pressure term which is treated fully implicitly. The PISO scheme (Issa, 1986) is used to deal with the pressure–velocity coupling between the momentum and the continuity equations. In order to avoid the check-board pressure field, the velocity interpolation method at the cell faces proposed by Rhie and Chow (1983) is employed.

A convective boundary condition $\partial\phi/\partial t + U_{\mathrm{conv}}(\partial\phi/\partial x) = 0$ (Sohankar et al., 1998) is used for the exit boundary, where U_{conv} is the convective velocity normal to the outlet boundary and ϕ is any physical variable convected out

through the outlet. No-slip boundary conditions are used for the top, bottom and cylinder walls. Periodic boundary conditions are applied in the spanwise direction. The normal derivative for the pressure correction is set to zero at all boundaries. The simulations start with a zero velocity and pressure field. The flow is allowed to develop for around 10 shedding periods and statistics are then collected for more than eight shedding cycles.

Fig. 2 shows a cross-section of the computational mesh used. In the experiments, the size of the domain in the spanwise direction was equal to $7.2D$ and was considered too large to simulate. In numerical calculations the spanwise length of the domain is usually estimated from prior knowledge of the size of the streamwise vortex structures. However, to the best of the authors' knowledge, correlations for the size of these structures are available only for steady approaching flow around a single cylinder and it is not clear how this size is affected by the presence of multiple cylinders. Moreover, it is difficult to extrapolate from other tube bundle simulations as the existing three-dimensional LES publications refer to the closely spaced array measured by Simonin and Barcouda (1988). Even for that geometry, the employed spanwise sizes differ significantly; for $\mathrm{Re} = 21\,700$, Hassan and Barsamian (2004) used a spanwise length of $5D$ and 37 layers while the DNS of Moulinec et al. (2004b) at $\mathrm{Re} = 6000$ was performed using $L_z = D$. In the present work, the total number of cells is equal to 785 920 distributed in 20 equally spaced layers that covered a spanwise length $L_z = \pi D$. This spanwise length is usually employed for single cylinder simulations.

Along the periphery of each cylinder 96 cells are placed. A constant expansion factor 1.16 is used for the cell spacings in the radial direction away from each cylinder wall. The smallest cell thickness in the radial direction is $\Delta r_{\min}/D = 1.8 \times 10^{-3}$, which is comparable to the finest mesh used in Beaudan and Moin (1994) ($\Delta r_{\min}/D = 1.25 \times 10^{-3}$) for a single cylinder at Reynolds number equal to 3900. The maximum cell size in the streamwise direction is located in between two successive cylinders and is equal to 0.72 mm. In the spanwise direction it is uniform and equal to 1.57 mm. The time step is equal to 0.15 ms. Around 20 iterations are required for convergence of the equations within each time step to within a prescribed tolerance of 10^{-3} for the normalised residuals. The simulations were carried out on a DELL Workstation 650, with Dual processor Xeon 3.06 GHz and 2 GB of RAM. The calculations were serial and take around 2 months in total (including the time for the flow to develop a steady vortex shedding pattern).

The temporal and spatial resolution can be also assessed against experimentally available time and length scales. Balabani and Yianneskis (1996) report that for $\mathrm{Re}_{\mathrm{gap}} = 12\,858$ the integral time scale is between 1.5 and 8 ms with an average value of 4 ms. In order to obtain these values, the velocity spectrum was filtered to remove any frequencies associated with the variation of mean flow due to large-scale vortex shedding. A notch filter was applied that was especially designed to remove only a narrow band around a specific frequency and therefore these values refer to high-frequency fluctuations that represent the real turbulence. The Taylor microscale was estimated to be in the region 0.4–2.2 ms with an average value of 0.7 ms. Note that the aforementioned values are expected to be higher for the examined Reynolds numbers of 8600. Therefore, the time step used for the integration of the Navier–Stokes equations is an order of magnitude smaller than the measured integral time scale of turbulence and is of the same order as the average Taylor microscale. Furthermore, using Taylor's hypothesis, Balabani and Yianneskis (1996) also report values for the integral (macro) and micro-length scales. The macroscale was in the region of 0.1–8.0 mm with an average value of 4.6 mm while the microscale was between 0.04 and 1.6 mm with an average value of 0.74 mm. Therefore, in the present calculations, the maximum cell size in the streamwise direction is very close to the average microscale, while in the spanwise direction is close to the maximum value.

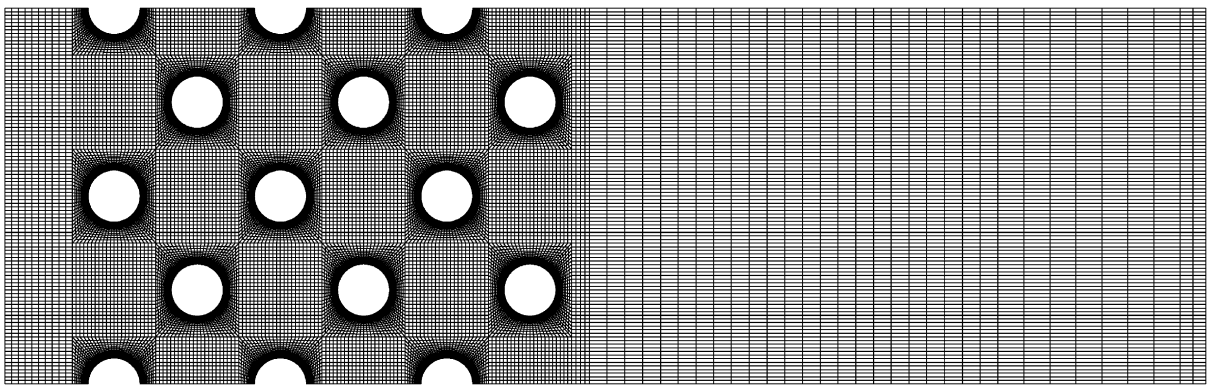

Fig. 2. Cross-section of the computational mesh of the six-row staggered tube bundle.

4. Results and discussion

In this section the results of the simulations will be presented and discussed. The first- and second-order statistics of the velocity will be compared with detailed experimental measurements in order to validate the methodology and subsequently the instantaneous features of the flow will be presented and discussed.

4.1. Time-averaged flow field

Detailed measurements for the streamwise and cross-stream mean and r.m.s. velocities at 17 stations along the depth of the array are available for Reynolds number $Re_{gap} = 12\,858$ only. For $Re_{gap} = 8600$ data are available for the streamwise velocity component (mean and r.m.s.) only for five stations between cylinders 1 and 2 (Castiglia et al., 2000) so the reliability of the LES predictions for the following cylinders cannot be assessed. The effect of Reynolds number on mean and r.m.s. velocities was examined by Balabani (1996) who performed measurements downstream of the first and third cylinder at Re_{gap} varying from 3104 to 12 858. Two correlations $l_r^1 = -0.76\log(Re_{gap}) + 4.66$ and $l_r^3 = -0.69\log(Re_{gap}) + 3.80$ for the variation of the size of recirculation zones with Re_{gap} behind the first and third cylinders, respectively, were provided. The length of each zone was measured from the centre of the corresponding cylinder. Table 1 summarises the predicted recirculation bubble sizes behind each tube and the results obtained from these correlations. The values of the experimental correlation for $Re_{gap} = 12\,858$ are also shown. It can be seen that the sizes of the zones of the first and third cylinder are in good agreement with the available correlations. Note also that the size is significantly affected by the location in the row; it is significantly smaller for the third cylinder. The effect of Reynolds number on the recirculation zone size is around 10%. Regarding turbulence quantities, it was found by Balabani (1996) that the maximum values of the streamwise r.m.s. velocity normalised by the bulk velocity behind the first and third cylinders were not affected significantly by variation of Reynolds number. This is due to the fact that very high values of turbulent intensity were measured: around 40–43% behind the first row and 52–55% behind the third row.

Fig. 3 shows detailed comparison between predictions and LDA measurements of Balabani and Yianneskis (1996) for the streamwise mean and r.m.s. velocities (normalised by the gap velocity). The uncertainty of experimental data is reported to be 1–5% and 5–10% for the mean velocity and turbulence quantities, respectively, with the higher errors occurring in regions of steep velocity gradients. Due to symmetry, only the distribution of velocities along the flow channel defined by cylinders 1–3–5 and 2–4–6 is shown (see Figs. 1 and 3(a) for cylinder numbering). The predicted streamwise mean velocity agrees very well with the measurements. The r.m.s. velocities also match well the measurement data at nearly all locations, apart from a small underprediction in the first row (first and second stations), which is due to the fact that turbulent fluctuations were not present in the simulations at the entrance of the domain. This figure shows clearly that turbulence is generated by the presence of cylinder walls and vortex shedding inside the array.

Fig. 4 shows good agreement between predictions and LDA measurements for the cross-wake mean and r.m.s. velocities. The r.m.s. of the transverse velocity is mainly due to vortex shedding. The small values of this quantity directly behind the first cylinder (compared to the rest of the cylinders in the bundle) indicates rather weak shedding activity behind this particular cylinder. Large values of r.m.s. velocity are noticed in front of cylinders 3, 4 and 5, the reason being the periodic vortex impingement from upstream cylinders as will be shown later on. The maximum value of r.m.s. velocity is found behind the second cylinder, at an area close to the front of the fourth cylinder. It is very gratifying that this is in agreement with the experimental observations of Balabani and Yianneskis (1996).

The previous comparison with the available experiments clearly demonstrates that the current grid resolution and solution method can predict with satisfactory accuracy the first- and second-order turbulence statistics. Having validated the numerical results, attention is now focused on the analysis of the instantaneous flow patterns.

Table 1
Recirculation bubble sizes: comparison between predictions and experimental correlations

Type	Re_{gap}	Tube 1	Tube 2	Tube 3	Tube 4	Tube 5
LES prediction	8600	1.66D	1.24D	1.1D	1.24D	1.15D
Experim. correlation	8600	1.67D	n/a	1.09D	n/a	n/a
Experim. correlation	12 858	1.53D	n/a	0.96D	n/a	n/a

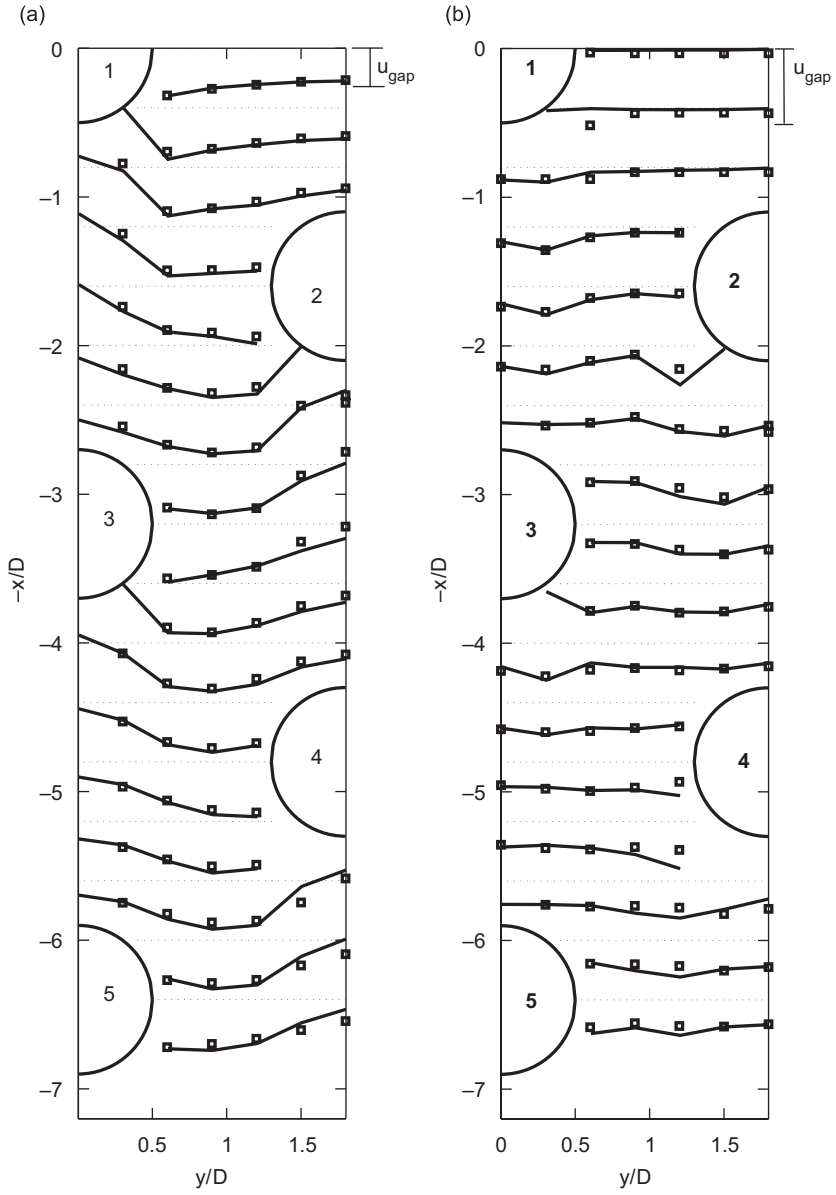

Fig. 3. Comparison between LES predictions (—) and measurements (□) at several stations for (a) mean and (b) r.m.s. streamwise velocities in a staggered tube bundle.

4.2. Analysis of the instantaneous flow field

Although the mean velocity field is two-dimensional, the instantaneous field at the examined Reynolds number is not. Fig. 5(a) shows the instantaneous velocity vectors around cylinder 3 in the (x, y) plane in the midspan of the domain. The vectors are colour-coded with the velocity magnitude in this plane i.e. with $\sqrt{\widetilde{u}^2 + \widetilde{v}^2}$. Fig. 5(b) shows a contour plot of the third velocity component ($\widetilde{w}$) at the same time instant. Positive and negative spots of spanwise velocity alternate in the z-direction with instantaneous values close to the velocity magnitude in the (x, y) plane. It becomes therefore clear that a fully three-dimensional simulation is necessary in order to capture the instantaneous features of this velocity field.

The variation of the instantaneous lift coefficient (C_L) for all cylinders against time is shown in Fig. 6. For the evaluation of the lift coefficient the bulk velocity is used. Other investigators [for example Oengören and Ziada (1998)]

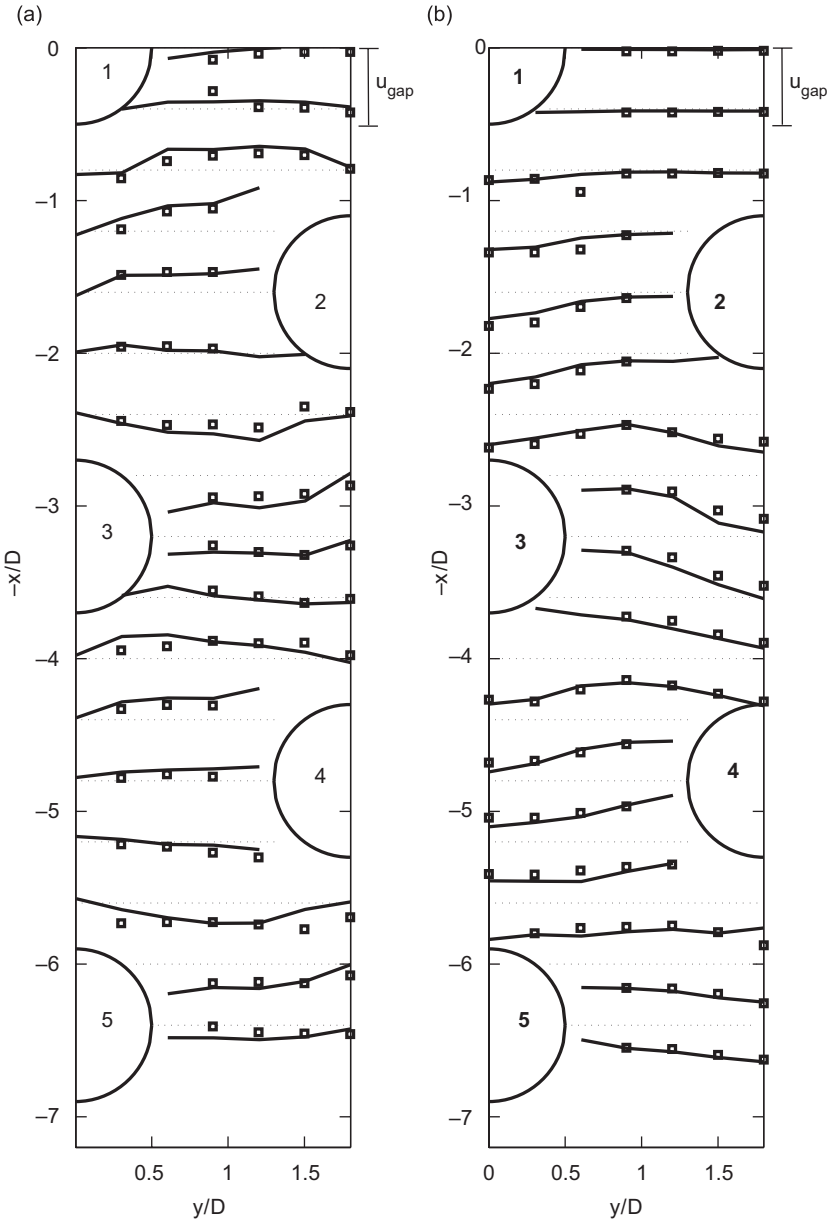

Fig. 4. Comparison between LES predictions (—) and measurements (□) at several stations for (a) mean and (b) r.m.s. cross-wake velocities in a staggered tube bundle.

use the gap velocity; with this velocity the lift coefficient is $1.385^2 = 1.92$ times smaller. It can be seen that the lift coefficient of the first cylinder does fluctuate but not much, indicating weak vortex shedding activity and this can explain the small values of the cross-stream r.m.s. velocities of Fig. 4(b) downstream of that cylinder as already mentioned. The maximum r.m.s. value of C_L (denoted as C'_L) is predicted for the third cylinder. The predicted values of C_L are larger compared with the reported values for a single cylinder (Norberg, 2003). It was not possible to find measurements of fluctuating forces for a similar arrangement in order to validate quantitatively the predictions. The actual r.m.s. values of C_L in tube bundles depend on the specific tube arrangement, the longitudinal and cross-stream tube spacings, the particular location of the examined cylinder inside the array and the reference velocity used for nondimensionalisation. Experimentally measured values larger than that of a single cylinder have been reported in a number of papers (Shim et al., 1988; Lam et al., 2003; Oengören and Ziada, 1998). Arrangements different from the

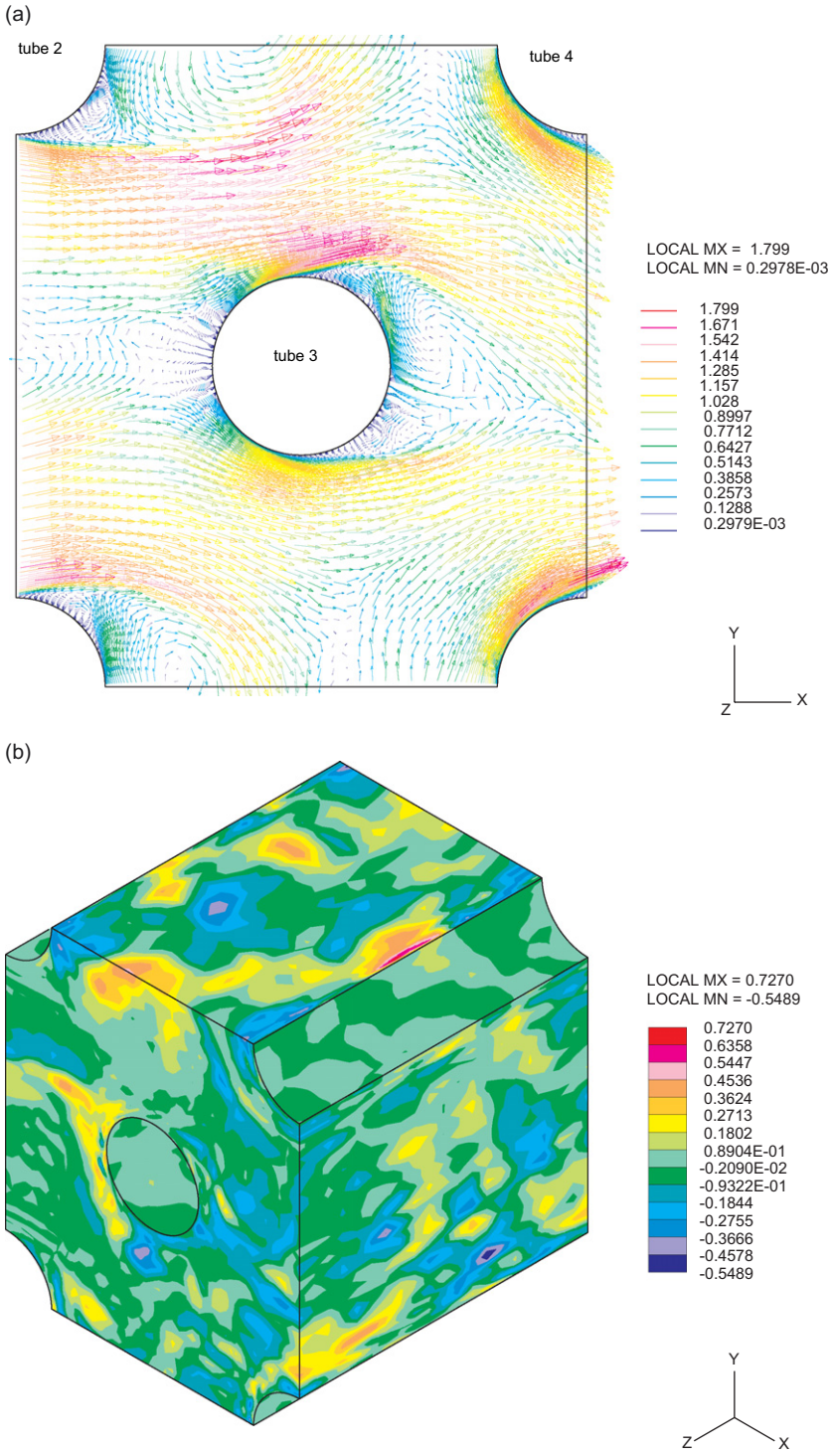

Fig. 5. Instantaneous flow field around cylinder 3: (a) velocity vectors (in m/s) in the middle x–y plane; (b) contour plots of spanwise velocity (the average gap velocity is 0.86 m/s).

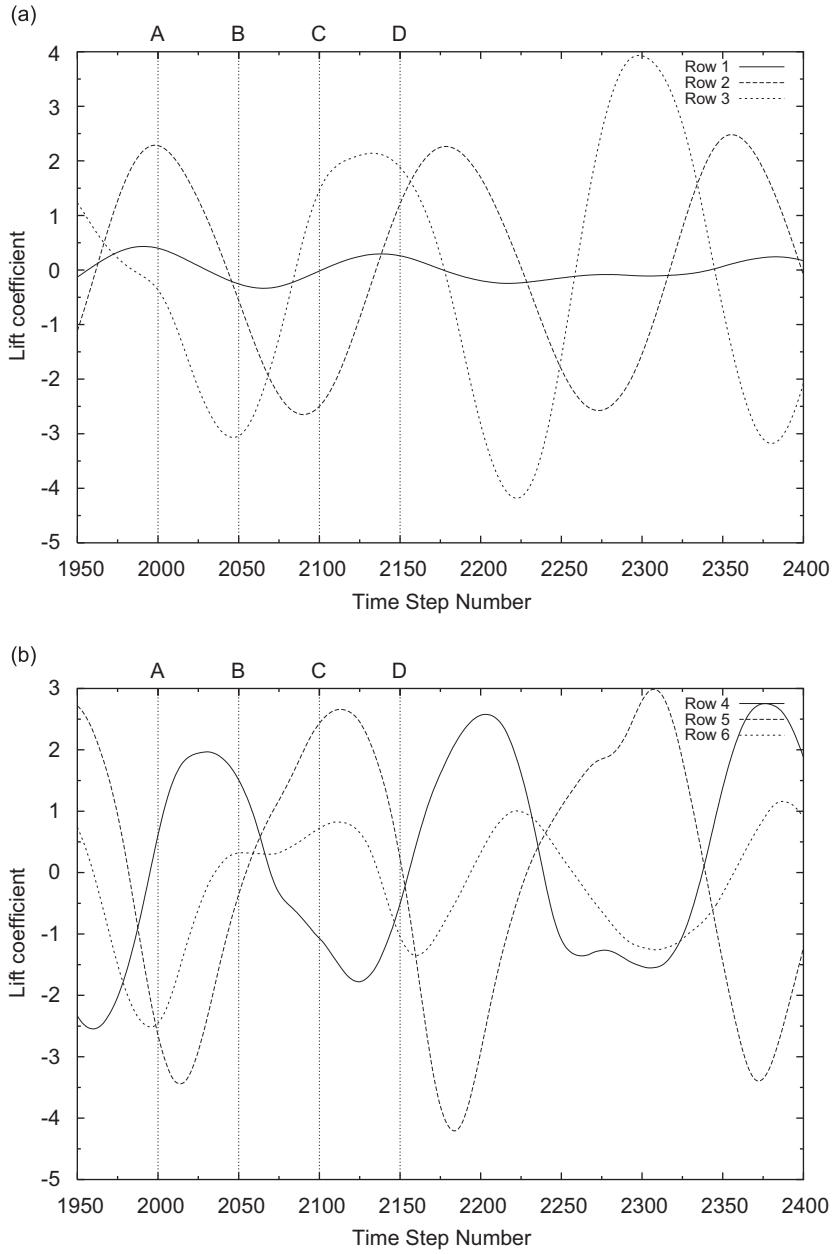

Fig. 6. Variation of lift coefficient for six cylinders. (a) 3 upstream rows (1-3); (b) 3 downstream rows (4-6).

present one have been examined but it seems that in all cases the largest value of C'_L is measured in the second or third row. Also the flow pattern plays a key role in the variation of the fluctuating forces. For example, when cylinders are continuously impinged by vortices shed by upstream cylinders, the C'_L increases significantly compared to a single cylinder, by a factor of 2 to more than 3 depending on the spacing ratio. On the other hand, cylinders in the first row have lower C'_L (Lam et al., 2003). All these findings are in agreement with the results of the present study. For Re equal to 10 000, which is close to the one examined in this paper, DNS results of Dong and Karniadakis (2005) for a flow around a single cylinder show maximum instantaneous C_L values in the region 0.7–0.9. Extrapolation of these values to cylinders impinged by vortices using the factor of Lam et al. (2003) leads to maximum C_L values close to the ones shown in Fig. 6. A second reason that may result in increased values of the predicted C'_L with respect to a free cylinder is the small number of cylinders in each row that makes the effect of the top and bottom channel walls important. There

are few studies on the effect of confinement ratio even for a single cylinder. For example, Richter and Naudascher (1976) and Kim et al. (2004) reported significantly increased values of C'_L compared to unconfined circular and square cylinders (prisms), respectively.

The four phases for which the velocity flow patterns were recorded and presented below are denoted in Fig. 6 with letters A–D. Instantaneous velocity vector plots colour-coded with the values of the instantaneous spanwise vorticity for these phases are shown in Fig. 7 for the first three rows and in Fig. 8 for the rest of the rows (4–6). It can be seen that the maximum vortex formation length is behind the first cylinder for all phases. The one behind the second cylinder is clearly shorter, which is consistent with the recirculation zone results of Table 1. This decrease in size is most probably related to the fact that the 'effective' Reynolds number is higher for cylinder 2 as the approaching velocity is the gap velocity (instead of the bulk) and is well known that in the examined Reynolds number regime the recirculation zone size decreases when the Reynolds number increases (Williamson, 1996). It must be borne in mind that this is an approximation since the jet flapping in the gap between cylinder 1 and the half-cylinder in the wall will affect the approaching flow to cylinder 2 but nevertheless on average the 'effective' Reynolds number will undoubtedly be higher compared to cylinder 1. This can also explain why the shedding activity is more intense behind the second cylinder compared to the first: since the formation length is smaller, there is plenty of space between cylinders 2 and 4 for the uninterrupted development and release of vortices.

Closer examination of the instantaneous flow patterns between cylinders 1 and 3 reveals that flow is in the 'vortex impinging' regime i.e. the Karman vortices shed by cylinder 1 impinge periodically on the front surface of cylinder 3. The same pattern also appears for the rest of the cylinder pairs that are located in the same column i.e. 2–4, 4–6, 3–5, etc. and can explain the large values of the cross-stream r.m.s. velocity in front of these cylinders. Unfortunately, flow visualisations are not available so comparisons of flow patterns cannot be made. However, it is very gratifying that Sumner et al. (2000), who studied experimentally the flow between a pair of cylinders, also observed this regime for small incidence angles ($0°-20°$) and pitch-to-diameter ratio 3–5 (the corresponding values for the arrangement examined here are $0°$ and $P/D = 3.2$ i.e. they fall within the aforementioned regions). The flow patterns behind rows 4–6 for the four phases A–D shown in Fig. 8 are clearly much more chaotic compared to rows 1–3, obviously due to the

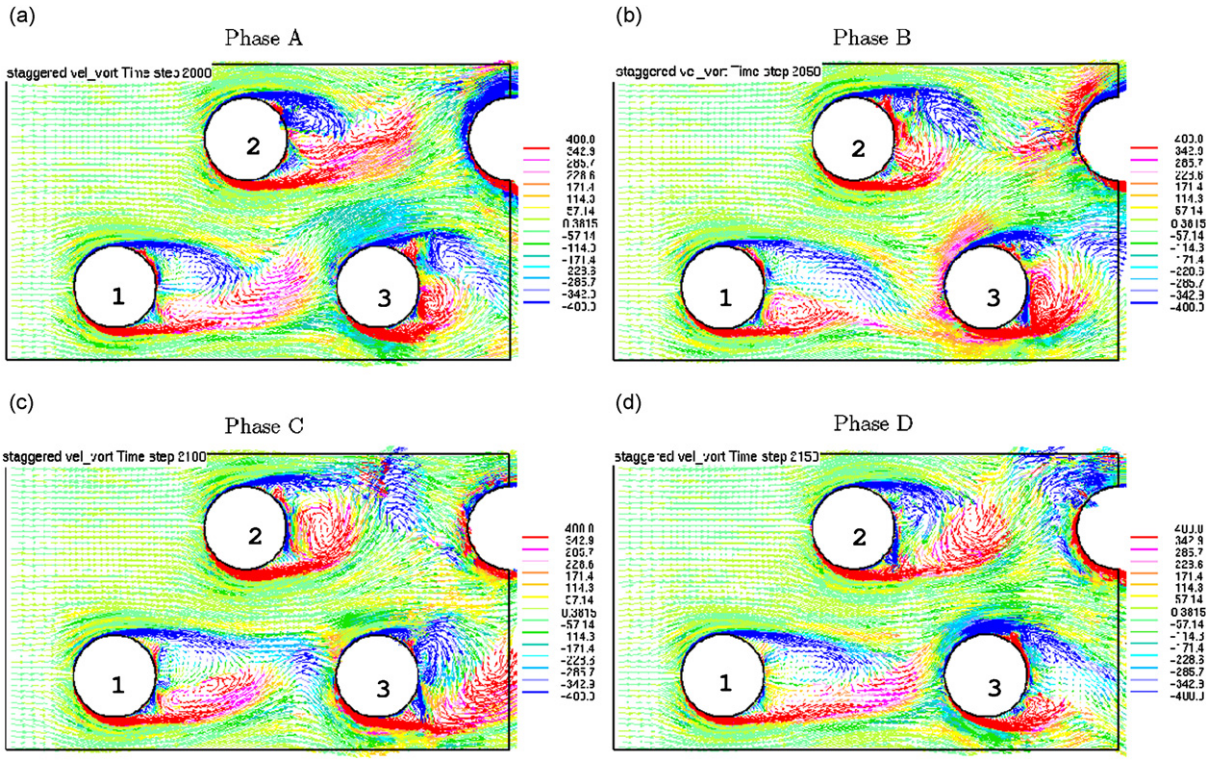

Fig. 7. Instantaneous velocity vectors at four time instants (phases A–D) colour-coded with the values of the instantaneous spanwise vorticity (rows 1–3).

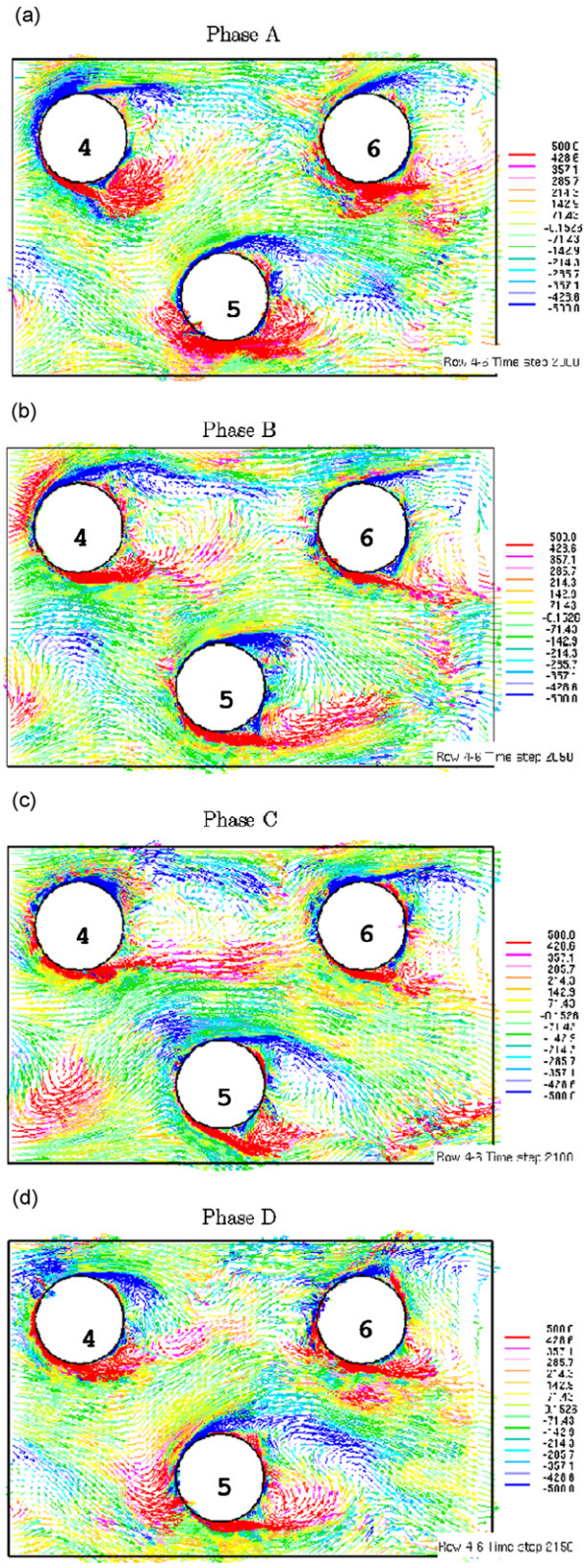

Fig. 8. Instantaneous velocity vectors at four time instants (phases A–D) colour-coded with the values of the instantaneous spanwise vorticity (rows 4–6).

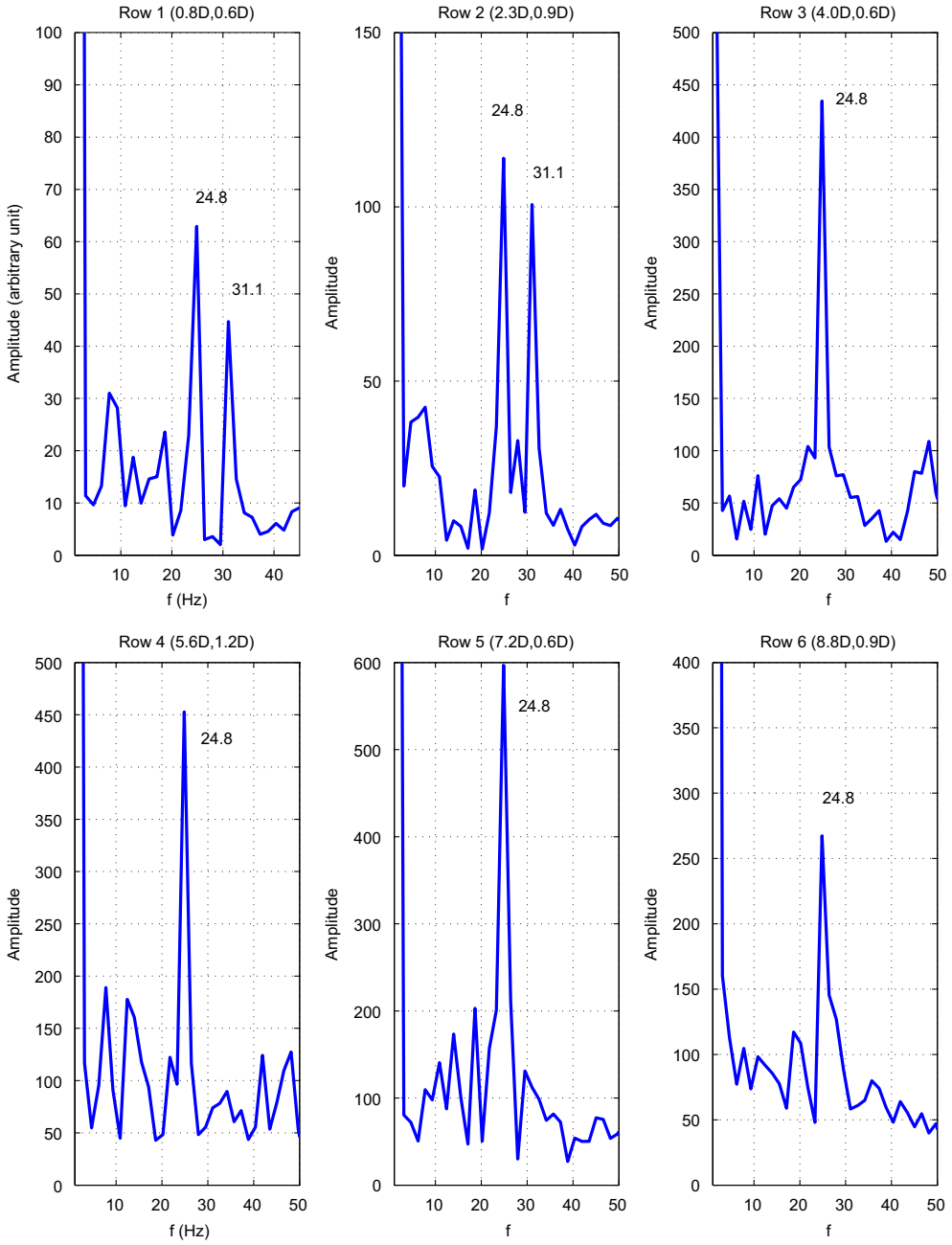

Fig. 9. Cross-wake velocity spectra of the steady cross-flow over the staggered tube bundle.

turbulence generated by the upstream rows. Therefore, it is much more difficult to analyse these fields but broad features, such as 'vortex impingement', can still be discerned.

Fig. 9 shows the cross-wake velocity frequency spectra at a point behind each row. For rows 1, 3 and 5 (i.e. for the middle column of cylinders), the monitoring point is located in the same relative position with respect to cylinder centre, $(0.8D, 0.6D)$, which is a position within the separating shear layer from the top of the cylinders. This allows a direct comparison between the spectra for those three cylinders. Note the sharp increase in the peak amplitude from cylinder 1 to 3 and the subsequent smaller increase between 3 and 5, which shows that the flow is approaching a periodic, repeatable, state. For row 2, the amplitude at the examined point is also small, although the lift coefficient shown in

Fig. 6 shows large variations. The reason for this difference is the fact that the examined point is not representative of the intensity of the vortex shedding process as it is not located within the shear layer of cylinder 2; in fact, it is located in the position ($0.7D$, $0.4D$) below the cylinder centre, i.e. further away from the wall and inside the free stream.

It is clear from Fig. 9 that two frequencies, 24.8 and 31.1 Hz, are detected behind the first and the second row, with the lower frequency persisting for all downstream rows. The corresponding Strouhal numbers (based on the gap velocity) are $St^1_{gap} = 0.28$ and $St^2_{gap} = 0.36$ (or $St^1_{bulk} = 0.38$ and $St^2_{bulk} = 0.49$ based on the bulk velocity). The value of Strouhal number corresponding to the smallest frequency (i.e. 0.28) agrees well with the experimental value of 0.26 of Balabani and Yianneskis (1996). However, a second, higher frequency was also observed in the present simulations in the first two front rows. Weaver et al. (1993), as already mentioned in the introduction, performed measurements of Strouhal number for rotated square arrays with pitch-to-diameter ratio $P/D = 1.21-2.83$. The examined arrangement approximates a rotated square to a good accuracy (the angle is 96° instead of 90°). The corresponding pitch ratio is 2.41 as already mentioned. For the very close pitch ratio of 2.42, Weaver et al. (1993) reported two Strouhal numbers of 0.37 and 0.51 (based on the bulk velocity) behind the first and the second row cylinders. These values are very close to the ones obtained from the present investigation. As already stated in the Introduction, multiple shedding frequencies have been measured in the past from several investigators. However, to the best of the authors' knowledge, this is the first time that successful reproduction of the second frequency using numerical simulation is reported. Therefore, it becomes now possible to examine in more detail the mechanisms responsible for the second frequency. Work on this is currently in progress and will be reported in a subsequent paper.

5. Closure

Most of the numerical simulations of the turbulent flow around tube bundles that have been performed to date either use the RANS approach or the LES technique applied on a periodic 'cell' in an arrangement with close tube spacings with weak vortex shedding. In addition, when flow across multiple rows is considered, most of the LES simulations are two-dimensional. In the present study, the aforementioned limitations were removed and full three-dimensional LES of the flow development in a staggered array consisting of six rows with intermediate tube spacings was performed at Reynolds number 8600.

Thorough validation against detailed experimental data showed that the basic turbulence statistics (mean and r.m.s. velocities) as well as the recirculation bubble lengths are in good agreement with measurements.

Two shedding frequencies were detected, in agreement with many experimental observations. While the low-frequency component was present behind all rows, the high component was detected behind the first and second rows only. Clearly, the fact that the flow was allowed to develop along multiple rows was instrumental for the successful prediction of these two shedding frequencies.

Acknowledgement

Chunlei Liang gratefully acknowledges the financial support of EPSRC (GR/ R04256/01) as well as ORS award. The authors would like to thank the reviewers for their comments which improved the paper.

References

Balabani, S., 1996. An experimental investigation of the crossflow over tube bundles. Ph.D. Thesis, King's College London, University of London.

Balabani, S., Yianneskis, M., 1996. An experimental study of the mean flow and turbulence structure of cross-flow over tube bundles. Proceedings of IMechE Part C, Journal of Mechanical Engineering Science 210, 317–331.

Balabani, S., Yianneskis, M., 1997. Vortex shedding and turbulence scales in staggered tube bundle flows. Canadian Journal of Chemical Engineering 75 (5), 823–831.

Barsamian, H.R., Hassan, Y.A., 1997. Large eddy simulation of turbulent crossflow in tube bundles. Nuclear Engineering and Design Journal 172, 103–122.

Beaudan, P., Moin, P., 1994. Numerical experiments on the flow past a circular cylinder at a subcritical Reynolds number. Technical Report TF-62. Thermosciences Division, Department of Mechanical Engineering, Stanford University.

Benhamadouche, S., Laurence, D., 2003. LES coarse LES, and transient RANS comparisons on the flow across a tube bundle. International Journal of Heat and Fluid Flow 24, 470–479.

Bouris, D., Bergeles, G., 1999. Two dimensional time dependent simulation of the subcritical flow in a staggered tube bundle using a subgrid scale model. International Journal of Heat and Fluid Flow 20, 105–114.

Butterworth, D., Guy, A.R., Welkey, J.J., 1996. Design and applications of twisted tube exchangers. In: Berryman, R.J. (Ed.), European Research Meeting on the Future Needs and Developments in Heat Exchanger Technology—Advances in Industrial Heat Transfer, IChemE, pp. 87–95.

Castiglia, D., Balabani, S., Yianneskis, M., 2000. Tabulated experimental results of flow pulsation and asymmetric tube arrangements investigated for minimisation of fouling, private communication.

Deardorff, J.W., 1970. A numerical study of three-dimensional turbulent channel flow at large Reynolds numbers. Journal of Fluid Mechanics 41, 453–480.

Dong, S., Karniadakis, G.E., 2005. DNS of flow past a stationary and oscillating cylinder at $Re = 10\,000$. Journal of Fluids and Structures 20, 519–531.

Hassan, Y.A., Barsamian, H.R., 1999. Turbulence simulation in tube bundle geometries using the dynamic subgrid-scale model. Nuclear Technology Journal 128, 58–74.

Hassan, Y.A., Barsamian, H.R., 2004. Tube bundle flows with the large eddy simulation technique in curvilinear coordinates. International Journal of Heat and Mass Transfer 47, 3057–3071.

Hassan, Y.A., Ibrahim, W.A., 1997. Turbulence prediction in two-dimensional bundle flows using large eddy simulation. Nuclear Technology Journal 119, 11–28.

Issa, R.I., 1986. Solution of the implicitly discretized fluid flow equations by operator splitting. Journal of Computational Physics 62, 40–65.

Kakac, S., Liu, H., 1997. Heat Exchangers: Selection, Rating and Thermal Design. CRC Press, Boca Raton, FL.

Kim, D.H., Yang, K.S., Senda, M., 2004. Large eddy simulation of turbulent flow past a square cylinder confined in a channel. Computers and Fluids 33, 81–96.

Konstantinidis, E., Castiglia, D., Balabani, S., Yianneskis, M., 2000. On the flow and vortex shedding characteristics of an inline tube bundle in steady and pulsating crossflow. Transactions of IChemE, Part A, Chemical Engineering Research and Design 78 (8), 1129–1138.

Lam, K., Li, J., So, R., 2003. Force measurements and Strouhal numbers of four cylinders in cross flow. Journal of Fluids and Structures 18, 305–324.

Lilly, D.K., 1977. The representation of small-scale turbulence in numerical simulation experiments. In: Goldstine, H.H. (Ed.), Proceedings IBM Scientific Computing Symposium on Environmental Sciences, York Town Heights, NY, pp. 195–210.

Moulinec, C., Hunt, J.C.R., Nieuwstadt, F.T.M., 2004a. Disappearing wakes and dispersion in numerically simulated flows through tube bundles. Flow, Turbulence and Combustion 73, 95–116.

Moulinec, C., Pourquié, M.J.B., Boersma, B.J., Buchal, T., Nieuwstadt, F.T.M., 2004b. Direct numerical simulation on a Cartesian mesh of the flow through a tube bundle. International Journal of Computational Fluid Dynamics 18, 1–14.

Norberg, C., 2003. Fluctuating lift on a circular cylinder: review and new measurements. Journal of Fluids and Structures 17, 57–96.

Oengören, A., Ziada, S., 1998. An in-depth study of vortex shedding, acoustic resonance and turbulent forces in normal triangle tube arrays. Journal of Fluids and Structures 12, 717–758.

Piomelli, U., Moin, P., Ferziger, J.H., 1988. Model consistency in large eddy simulation of turbulent channel flows. Physics of Fluids 31, 1884–1891.

Polak, D.R., Weaver, D.S., 1995. Vortex shedding in normal triangular tube arrays. Journal of Fluids and Structures 9, 1–17.

Price, J.S., Païdoussis, M.P., Mark, B., 1995. Flow visualisation of the interstitial cross-flow through parallel triangular and rotated square arrays of cylinders. Journal of Sound and Vibration 181, 85–98.

Rhie, C.M., Chow, W.L., 1983. Numerical study of the turbulent flow past an airfoil with trailing edge separation. AIAA Journal 21, 1525–1532.

Richter, A., Naudascher, E., 1976. Fluctuating forces on a rigid circular cylinder in confined flow. Journal of Fluid Mechanics 78, 561–576.

Rollet-Miet, P., Laurence, D., Ferziger, J.H., 1999. LES and RANS of turbulent flow in tube bundles. International Journal of Heat and Fluid Flow 20, 241–254.

Sagaut, P., 2002. Large Eddy Simulation for Incompressible Flows: An Introduction. Springer, Berlin.

Shim, K., Hill, R., Lewis, R., 1988. Fluctuating lift forces and pressure distributions due to vortex shedding in tube banks. International Journal of Heat and Fluid Flow 9 (2), 131–146.

Simonin, O., Barcouda, M., 1988. Measurements and prediction of turbulent flow entering a staggered tube bundle. In: Proceedings of Fourth International Symposium on Applications of Laser Anemometry to Fluid Mechanics, Lisbon, paper number 5.23.

Smagorinsky, J., 1963. General circulation experiments with the primitive equations. i. The basic experiment. Monthly Weather Review 91, 99–164.

Sohankar, A., Norberg, C., Davidson, L., 1998. Low-Reynolds flow around a square cylinder at incidence: study of blockage, onset of vortex shedding and outlet boundary condition. International Journal for Numerical Methods in Fluids 26, 39–56.

Sumner, D., Price, S.J., Païdoussis, M.P., 2000. Flow-pattern identification for 2 staggered circular cylinders in cross-flow. Journal of Fluid Mechanics 411, 263–303.

Weaver, D.S., Lian, H.Y., Huang, X.Y., 1993. Vortex shedding in rotated square arrays. Journal of Fluids and Structures 7, 107–121.

Williamson, C.H.K., 1996. Vortex dynamics in the cylinder wake. Annual Review of Fluid Mechanics 28, 477–539.

Ziada, S., Oengören, A., 1992. Vorticity shedding and acoustic resonance in an inline tube bundle. Part I: vorticity shedding. Journal of Fluids and Structures 6, 271–292.

Ziada, S., Oengören, A., 1993. Vortex shedding in an inline tube bundle with large tube spacings. Journal of Fluids and Structures 7, 661–687.

Ziada, S., Oengören, A., 2000. Flow periodicity and acoustic resonance in parallel triangle tube bundles. Journal of Fluids and Structures 14, 197–219.